**DEVCOM**
ARMY RESEARCH
LABORATORY

# Electroconducting Sphere inside Unbounded Isotropic Matrix for ALEGRA Verification

by Michael Grinfeld, Pavel Grinfeld, John Niederhaus, and Angel Rodriguez

**NOTICES**

**Disclaimers**

The findings in this report are not to be construed as an official Department of the Army position unless so designated by other authorized documents.

Citation of manufacturer's or trade names does not constitute an official endorsement or approval of the use thereof.

Destroy this report when it is no longer needed. Do not return it to the originator.

# Electroconducting Sphere inside Unbounded Isotropic Matrix for ALEGRA Verification

**Michael Grinfeld**
*Weapons and Materials Research Directorate, CCDC Army Research Laboratory*

**Pavel Grinfeld**
*Drexel University*

**John Niederhaus and Angel Rodriguez**
*Sandia National Laboratories*

# REPORT DOCUMENTATION PAGE

| 1. REPORT DATE *(DD-MM-YYYY)* | 2. REPORT TYPE | 3. DATES COVERED (From - To) |
|---|---|---|
| July 2020 | Technical Report | 1 November 2019–1 June 2020 |

| 4. TITLE AND SUBTITLE | 5a. CONTRACT NUMBER |
|---|---|
| Electroconducting Sphere inside Unbounded Isotropic Matrix for ALEGRA Verification | |
| | 5b. GRANT NUMBER |
| | 5c. PROGRAM ELEMENT NUMBER |
| 6. AUTHOR(S) | 5d. PROJECT NUMBER |
| Michael Grinfeld, Pavel Grinfeld, John Niederhaus, and Angel Rodriguez | |
| | 5e. TASK NUMBER |
| | 5f. WORK UNIT NUMBER |

| 7. PERFORMING ORGANIZATION NAME(S) AND ADDRESS(ES) | 8. PERFORMING ORGANIZATION REPORT NUMBER |
|---|---|
| CCDC Army Research Laboratory<br>ATTN: FCDD-RLW-PA<br>Aberdeen Proving Ground, MD 21005 | ARL-TR-8994 |

| 9. SPONSORING/MONITORING AGENCY NAME(S) AND ADDRESS(ES) | 10. SPONSOR/MONITOR'S ACRONYM(S) |
|---|---|
| | |
| | 11. SPONSOR/MONITOR'S REPORT NUMBER(S) |

**12. DISTRIBUTION/AVAILABILITY STATEMENT**

Approved for public release; distribution is unlimited.

**13. SUPPLEMENTARY NOTES**

**14. ABSTRACT**

This report analyzes a nonlinear electroconducting sphere embedded in an unbounded linear isotropic matrix with a prescribed linear electric current at infinity. The exact analytical solution of this problem is reduced to solving a nonlinear algebraic equation. For the linear conductor we arrive at the explicit solution, which can be recommended for the verification purposes of ALEGRA code. The ALEGRA solution for one realization of the problem is shown to agree with the analytical solution to within a tiny fraction of the far-field values.

**15. SUBJECT TERMS**

electromagnetism, stationary electric current, exact analytical solution, code verification, ALEGRA implementation

| 16. SECURITY CLASSIFICATION OF: | | | 17. LIMITATION OF ABSTRACT | 18. NUMBER OF PAGES | 19a. NAME OF RESPONSIBLE PERSON |
|---|---|---|---|---|---|
| a. REPORT | b. ABSTRACT | c. THIS PAGE | UU | 31 | Michael Grinfeld |
| Unclassified | Unclassified | Unclassified | | | 19b. TELEPHONE NUMBER (Include area code)<br>410-278-3070 |

# Contents

## List of Figures

## Acknowledgments

# 1. Introduction

The ALEGRA[*] software is used heavily in engineering research and development efforts. Its technical credibility relies on rigorous verification efforts, which, in turn, rely on the discovery and/or development of analytic solutions for the physics equations that ALEGRA solves numerically, in problems that are relevant to engineering needs. Engineers must deal with quite complex systems, characterized by numerous material parameters, sophisticated geometrical shapes of different parts, interfaces of different physical nature, and wide ranges of physical parameters, requiring essentially nonlinear equations of state or kinetics equations.

Of course, it is an advantage that computer-based modeling allows synthesis of multiple effects in a coherent project. It is clear, however, that exact analytical solutions for real engineering systems are simply unthinkable. The only realistic approach to the verification consists of applying the ALEGRA code to the relevant subsystems of the original system. If the subsystem is sufficiently simple there appears a chance not only to generate exact analytical solutions and compare them with the results, delivered by ALEGRA, but also to explore the rate of convergence of the ALEGRA-generated solutions to the explicit solutions.

With the wide implementation of the computer-based approaches in the engineering practice the role of analytical solutions essentially changes. On the first glance, the role of analytical solutions diminishes, and some engineers think the role of those solutions becomes negligible. This vision has nothing in common with reality. In fact, computers do, basically, more or less routine work that allows analytically minded researchers to concentrate on the most difficult qualitative aspects of the phenomena under study. Also, in some domains it is necessary to combine numerical solutions in the subdomains that have slow-varying fields with analytical solutions in the vicinity of domains that have extremely fast rates of change of the fields of interest.

In this and forthcoming reports we deal with modeling propagation of electric current in heterogeneous media. The heterogeneities may have different origins. For instance, they can have deliberately designed origins. Such engineering materials are called composite materials. For instance, we may deal with a nonconducting ceramic matrix containing highly conducting metal parts in the form of rods or spheres. Also, the heterogeneities can appear under the influence of heating, generated within the originally uniform electroconducting matrix due to the Ohm's heating. The heating is able to create subdomains of the completely melted and even evaporated materials. Those subdomains dramatically change their

---

[*] Arbitrary Lagrangian-Eulerian General Research Application

1

conductivity when undergoing melting or evaporations. Such materials are of a big interest in applied—in particular, military systems (see, for instance, Cooper[1] and Hansen[2]). Our main target are the systems, including mechanisms similar to the exploding wires.

Exploding wires have been intensively explored with the help of ALEGRA.[3,4] This technology includes a variety of different phenomena: phase transformations, plasma generation, and electromagnetism, among others. A significant feature of those phenomena are remarkably high deformation rates and very short time scale. Nevertheless, we will begin our verification work examining ALEGRA in the simplest case, when dealing with the steady state current. In this first report, we concentrate on the case of a spherical conductor. In the second one we will extend our analysis for a much bigger variety of the shapes, which can be approximated with the triaxial ellipsoids. Mathematically, this problem is quite close to the problems analyzed in many advanced textbooks on mathematical physics and applications to hydrodynamics, electrodynamics,[5] the Newtonian potential theory,[6] and heat conduction,[7] among many others. In this report, we use a method that can be traced back to the papers of Eshelby.[8,9] One of the advantages of this method is it permits the extension for the inclusions with nonlinear Ohm's law. This extension is particularly important for engineering applications dealing with electric currents of hundreds of thousands of amperes.

Earlier, we implemented the Eshelby technique in ALEGRA treatments of magnetization problems.[10,11] Here, it is implemented in a different context for studying electrification and Ohmic heating (also called "resistive" or "Joule" heating) in heterogeneous material. The specific problem we consider is described in Section 2, involving electrification of an inclusion within some conducting matrix. This problem provides several of the desired features for a challenging verification problem, including the presence of multiple materials and interfaces among them that have nontrivial shapes. Elliott and Larsson analyzed the problem of Joule heating, but only for a single-material domain.[12] Rienstra studied Joule heating in a material with insulating boundaries, but the boundaries had a corner, resulting in a singularity.[13] Here, we study an inclusion with a circular shape, which allows for a simpler solution form that can be used for verification of numerical methods. Exact solutions for this problem, including linear and nonlinear materials, are derived in Section 3 for a spherical inclusion and in Section 4 for a cylindrical inclusion. Two limiting cases are considered in Section 5 for the spherical inclusion shape and linear materials: a conducting inclusion and an insulating inclusion. For these two cases, the analytic solution is evaluated and plotted for visualization. Section 6 describes the setup of an ALEGRA simulation for the insulating case and,

finally, Section 7 shows ALEGRA simulation results for the problem, with quantitative comparison to the analytic solution.

## 2.    Mathematical Formulation of the Problem

Consider a spherical conductor embedded in an infinite conducting space, as shown in Fig. 1. Let $\Omega_+$ be the domain inside the inclusion and $\Omega_-$ be the domain outside the inclusion. The electrostatic potential $\varphi$ satisfies the Laplace equation everywhere (inside and outside the inclusion)

$$\nabla_i \nabla^i \varphi = 0 \qquad . \tag{1}$$



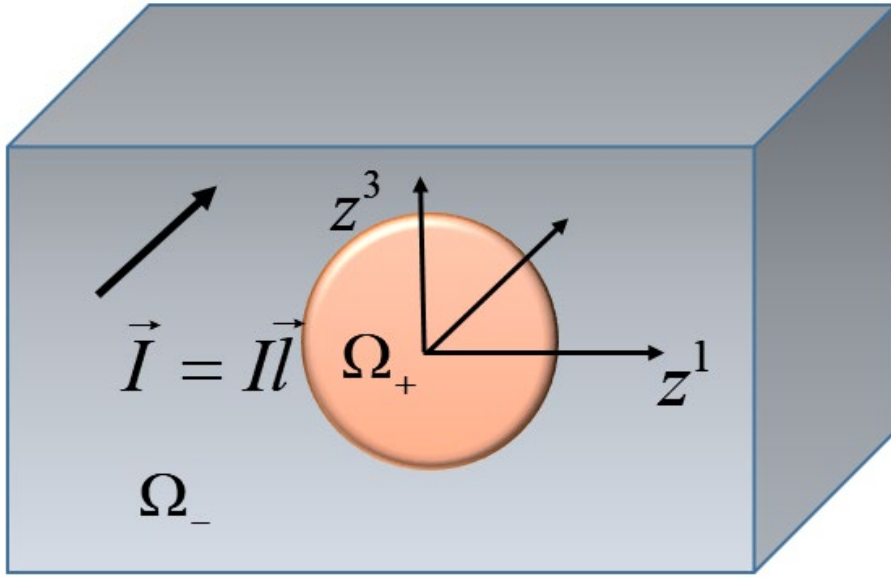**Fig. 1    Conducting inclusion within conducting matrix**

At the boundary $S$ the following conditions should be satisfied:

$$[\varphi]_-^+ = 0 \tag{2}$$

and

$$[I_i]_-^+ N^i = 0 \tag{3}$$

where $I_i$ is the component of the electric current and $N^i$ are the components of the normal to the boundary.

At infinity, we use the following condition

$$I_i(z) \to I l_i \text{ at } |z^i| \to \infty \tag{4}$$

where $I$ is a constant and $l_i$ is the field of parallel unit vectors.

It is assumed the matrix is made of a linear isotropic conductor; this means the current $I^i$ is connected with the potential gradient $\nabla_i \varphi$ via the classical Ohm's law

$$I_i = -\sigma_{mat} \nabla_i \varphi \tag{5}$$

where $\sigma_{mat}$ is a positive constant called the conductivity.

We assume a much more general conductivity law inside the inclusion

$$I_i = F_i(\nabla_m \varphi) \tag{6}$$

where $F_i$ is an arbitrary vector-function of the gradient of the electrostatic potential.

When $F_i$ is a linear vector-function, we get

$$F_i(\nabla_m \varphi) = -\sigma_{ij} \nabla^j \varphi \tag{7}$$

where $\sigma_{ij}$ is the conductivity tensor. It is usually assumed (using different arguments) this tensor is positive definite and symmetric. When the matrix is isotropic we get, by definition,

$$\sigma_{ij} = \sigma_{inc} z_{ij} \tag{8}$$

and Eqs. 6 and 7 lead to the standard Ohm's law

$$I_i = -\sigma_{inc} \nabla_i \varphi \tag{9}$$

where (in Eq. 8) $z_{ij}$ is the metrics coinciding with the Kronekker delta in the Cartesian coordinates).

In this case, we can rewrite the current continuity boundary condition Eq. 3 in the form

$$\sigma_{mat} \nabla_i \varphi N^i = \sigma_{inc} \nabla_i \varphi N^i \qquad . \tag{10}$$

However, in general, we neither need the assumption of isotropy or linearity of the inclusion. In this general situation, the boundary condition of the current continuity reads

$$\sigma_{mat} \nabla_i \varphi N^i = F_i(\nabla_m \varphi) N^i \tag{11}$$

where $\Phi(|\nabla \varphi|)$ is a certain function of the module of the potential gradient.

When the inclusion is isotropic but still nonlinear, we get

4

$$F_i(\nabla_m \varphi) = \Phi(|\nabla\varphi|)\nabla_i \varphi \quad . \tag{12}$$

When the inclusion is isotropic but still nonlinear, the Eq. 11 should be replaced with the following one:

$$\sigma_{mat}\nabla_i \varphi N^i = \Phi(|\nabla\varphi|)\nabla_i \varphi N^i \quad . \tag{13}$$

In the case of a linear isotropic inclusion, we get

$$\Phi(|\nabla\varphi|) = \sigma_{inc} \quad . \tag{14}$$

## 3.   Exact Solution for Spherical Inclusion

We will be looking for the solution in the following form:

$$\varphi_{mat}(z) = \left(A_i \frac{1}{r^3} - \frac{I}{\sigma_{mat}} l_i\right) z^i \quad \text{outside the sphere} \tag{15}$$

and

$$\varphi_{inc}(z) = K_i z^i \quad \text{inside the sphere} \quad . \tag{16}$$

The linear function $\varphi_{inc}(z)$ obviously satisfies the Laplace Eq. 1.

Let us demonstrate now that the function $\varphi_{mat}(z)$ also satisfies the Laplace equation. Indeed, we get

$$\nabla_i \varphi_{mat}(z) = A_i \frac{1}{r^3} - \frac{I}{\sigma_{mat}} l_i - 3A_m \frac{1}{r^5} z^m z^k z_{ik} \tag{17}$$

and

$$\nabla_j \nabla_i \varphi_{mat}(z) = -3A_i \frac{1}{r^5} z_{mj} z^m - 3A_j \frac{1}{r^5} z^k z_{ik} - 3A_m \frac{1}{r^5} z^k z_{ij}$$
$$+15A_m \frac{1}{r^7} z^m z^k z_{ik} z_{jn} z^n \quad . \tag{18}$$

Using Eq. 18, we get

$$\nabla^i \nabla_i \varphi_{mat}(z) = -3A_i \frac{1}{r^5} z^i - 3A_j \frac{1}{r^5} z^i - 9A_m \frac{1}{r^5} z^m + 15A_m \frac{1}{r^5} z^m z^k = 0 \quad . \tag{19}$$

It is easy to see the function Eq. 15 satisfies the condition Eq. 4 at infinity.

To solve the boundary value problem, it remains to satisfy the boundary conditions Eqs. 2 and 11.

With the help of the relationships Eqs. 16 and 17 the condition Eq. 2 of the potential continuity can be rewritten as

$$\left( A_i \frac{1}{r^3} - \frac{I}{\sigma_{mat}} l_i - K_i \right) z^i = 0 \quad . \tag{20}$$

The boundary condition Eq. 20 will be satisfied at all points of the boundary interface $z^i z^i z_{ij} = R^2$ if the following relationship is satisfied:

$$A_i \frac{1}{R^3} - K_i = \frac{I}{\sigma_{mat}} l_i \quad . \tag{21}$$

With the help of the relationships Eqs. 16 and 17, the flux-continuity boundary condition Eq. 11 can be rewritten as

$$\sigma_{mat} \left( A_i \frac{1}{r^3} - \frac{I}{\sigma_{mat}} l_i - 3A_m \frac{1}{r^5} z^m z^k z_{ik} \right) N^i = F_i(K_m) N^i \quad . \tag{22}$$

Using the relationship $N^i = (1/R) z^i$, we can rewrite the boundary condition Eq. 22 as

$$\sigma_{mat} \left( A_i \frac{1}{R^3} - \frac{I}{\sigma_{mat}} l_i - 3A_m \frac{1}{R^5} z^m z^k z_{ik} \right) z^i = F_i(K_m) z^i \quad . \tag{23}$$

After simple regrouping and adding similar terms we can rewrite Eq. 23 as

$$\sigma_{mat} \left( 2A_i \frac{1}{R^3} + \frac{I}{\sigma_{mat}} l_i \right) z^i = -F_i(K_m) z^i \quad . \tag{24}$$

The relationship Eq. 24 will be satisfied in all points of the inclusion's boundary if the following relationship holds:

$$\sigma_{mat} \left( 2A_i \frac{1}{R^3} + \frac{I}{\sigma_{mat}} l_i \right) = -F_i(K_m) \quad . \tag{25}$$

Thus, we arrive at the system of two vectorial algebraic equations, 21 and 25, for two unknown vectors, $A_i$ and $K_i$.

In the case of a nonlinear isotropic inclusion we use the relationships Eqs. 12 and 13. We then replace Eq. 25 with

$$\sigma_{mat} \left( 2A_i \frac{1}{R^3} + \frac{I}{\sigma_{mat}} l_i \right) = -\Phi(|K_m|) K_i \quad . \tag{26}$$

Eliminating $A_i$ between Eqs. 21 and 26, we get

$$\sigma_{mat} \left( \left( \frac{2}{\sigma_{mat}} + \frac{1}{\sigma_{mat}} \right) I l_i + 2K_i \right) = -\Phi(|K_m|) K_i \tag{27}$$

or

$$\left(\frac{1}{\sigma_{mat}}\Phi(|K_m|)+2\right)K_i = -I\frac{3}{\sigma_{mat}}l_i \quad . \tag{28}$$

For the linear isotropic inclusion we get, combining Eqs. 14 and 28,

$$\left(\frac{\sigma_{inc}}{\sigma_{mat}}+2\right)K_i = -\frac{3}{\sigma_{mat}}Il_i \quad . \tag{29}$$

Equation 29 implies

$$K_i = -\frac{3}{\sigma_{inc}+2\sigma_{mat}}Il_i \quad . \tag{30}$$

Inserting Eq. 30 in Eq. 21, we get

$$A_i = R^3\frac{\sigma_{inc}-\sigma_{mat}}{\sigma_{mat}(\sigma_{inc}+2\sigma_{mat})}Il_i \quad . \tag{31}$$

Summarizing Eqs. 15, 16, 30, and 31, we arrive at the following exact solution:

$$\varphi_{mat}(z) = \left(\frac{\sigma_{inc}-\sigma_{mat}}{\sigma_{inc}+2\sigma_{mat}}\frac{R^3}{r^3}-1\right)\frac{1}{\sigma_{mat}}Il_iz^i \quad \text{outside the sphere} \tag{32}$$

and

$$\varphi_{inc}(z) = -\frac{3}{\sigma_{inc}+2\sigma_{mat}}Il_iz^i \quad \text{inside the sphere} \quad . \tag{33}$$

The relationships Eqs. 32 and 33 imply the following relationships for the electric field $E_i = -\nabla_i\varphi$:

a) outside the sphere:

$$E_{i_{mat}}(z) = -\left(\frac{\sigma_{inc}-\sigma_{mat}}{\sigma_{inc}+2\sigma_{mat}}\frac{R^3}{r^3}-1\right)\frac{1}{\sigma_{mat}}l_iI + 3\frac{\sigma_{inc}-\sigma_{mat}}{\sigma_{inc}+2\sigma_{mat}}\frac{R^3}{r^5}z_{im}z^mz^k\frac{1}{\sigma_{mat}}Il_k \tag{34}$$

b) inside the sphere:

$$E_{i_{inc}}(z) = \frac{3}{\sigma_{inc}+2\sigma_{mat}}Il_i \quad . \tag{35}$$

For the current we get the relationship

a) outside the sphere:

$$I_{i_{mat}}(z) = \left(1-\frac{\sigma_{inc}-\sigma_{mat}}{\sigma_{inc}+2\sigma_{mat}}\frac{R^3}{r^3}\right)l_iI + 3\frac{\sigma_{inc}-\sigma_{mat}}{\sigma_{inc}+2\sigma_{mat}}\frac{R^3}{r^5}z_{im}z^mz^kIl_k \tag{36}$$

b) inside the sphere:

$$I_{iinc}(z) = \frac{3\sigma_{ink}}{\sigma_{inc}+2\sigma_{mat}} I l_i \quad . \tag{37}$$

In the case of nonconducting inclusion, when $\sigma_{inc} = 0$, the relationships Eqs. 36 and 37 imply

a) outside the sphere:

$$\frac{I_{i_{mat}}(z)}{I} = \left(1 + \frac{1}{2}\frac{R^3}{r^3}\right) l_i - \frac{3}{2}\frac{R^3}{r^5} z_{im} z^m z^k l_k \tag{38}$$

b) inside the sphere:

$$I_{i_{inc}}(z) = 0 \quad . \tag{39}$$

For the current $I_{rad}(r)$ in the matrix along the line pointed to the center of the sphere, the relationship Eq. 38 implies the following formula:

$$I_{rad}(r) = I^i l_i = \left(1 - \frac{R^3}{r^3}\right) I \quad . \tag{40}$$

In the case of superconducting inclusion, when $\sigma_{inc} = \infty$, the relationships Eqs. 36 and 37 imply

a) outside the sphere:

$$\frac{I_{i_{mat}}(z)}{I} = \left(1 - \frac{R^3}{r^3}\right) l_i + 3\frac{R^3}{r^5} z_{im} z^m z^k l_k \tag{41}$$

b) inside the sphere:

$$\frac{I^i_{inc}(z)}{I} = 3l^i \quad . \tag{42}$$

Also, the relationship Eq. 33 implies in the superconducting case

$$\varphi_{inc}(z) = 0 \quad \text{inside the sphere} . \tag{43}$$

## 4.  Exact Solution for the 2-D Problem

For the 2-D problem about a circular inclusion inside an infinite isotropic matrix we are looking for the exact solution in the form:

$$\varphi_{mat}(z) = \left(a_i \frac{1}{r^2} - \frac{I}{\sigma_{mat}} l_i\right) z^i \quad \text{outside the circular inclusion} \tag{44}$$

and

8

$$\varphi_{inc}(z) = k_i z^i \quad \text{inside the circle .} \tag{45}$$

We proceed as follows:

$$\nabla_i \varphi_{mat}(z) = a_i \frac{1}{r^2} - \frac{I}{\sigma_{mat}} l_i - 2A_m \frac{1}{r^4} z^m z^k z_{ik} \tag{46}$$

and

$$\nabla_j \nabla_i \varphi_{mat}(z) = -2a_i \frac{1}{r^4} z_{mj} z^m - 2a_j \frac{1}{r^4} z^k z_{ik} - 2a_m \frac{1}{r^4} z^k z_{ij}$$
$$+ 8a_m \frac{1}{r^6} z^m z^k z_{ik} z_{jn} z^n \quad . \tag{47}$$

Using Eq. 47, we get

$$\nabla^i \nabla_i \varphi_{mat}(z) = 0 \quad . \tag{48}$$

The boundary condition Eq. 6 remains unchanged

$$a_i \frac{1}{R^2} - k_i = \frac{I}{\sigma_{mat}} l_i \quad . \tag{49}$$

The flux continuity condition Eq. 21 should be replaced with the following one:

$$\sigma_{mat} \left( a_i \frac{1}{r^2} - \frac{I}{\sigma_{mat}} l_i - 2a_m \frac{1}{r^4} z^m z^k z_{ik} \right) N^i = F_i(k_m) N^i \tag{50}$$

whereas Eq. 23 should be replaced with

$$\sigma_{mat} \left( a_i \frac{1}{r^2} - \frac{I}{\sigma_{mat}} l_i - 2a_m \frac{1}{r^4} z^m z^k z_{ik} \right) z^i = F_i(k_m) z^i \tag{51}$$

or

$$\sigma_{mat} \left( a_i \frac{1}{R^2} + \frac{I}{\sigma_{mat}} l_i \right) = -F_i(k_m) \quad . \tag{52}$$

In the case of a linear isotropic inclusion, the Eq. 24 should be replaced with the following one:

$$\sigma_{mat} \left( a_i \frac{1}{R^2} + \frac{I}{\sigma_{mat}} l_i \right) = -\sigma_{inc} k_i \quad . \tag{53}$$

Eliminating $a_i$ between Eqs. 49 and 53, we get

$$\sigma_{mat} \frac{2I}{\sigma_{mat}} l_i = -(\sigma_{inc} + \sigma_{mat}) k_i \tag{54}$$

and then

$$k_i = -\frac{\sigma_{mat}}{\sigma_{inc}+\sigma_{mat}}\frac{2I}{\sigma_{mat}}l_i \quad . \tag{55}$$

Inserting Eqs. 55 in 49, we get

$$a_i = R^2 \frac{\sigma_{inc}-\sigma_{mat}}{\sigma_{inc}+\sigma_{mat}}\frac{I}{\sigma_{mat}}l_i \quad . \tag{56}$$

Combining Eqs. 44, 45, 55, and 56, we arrive at the following exact solution:

$$\varphi_{mat}(z) = \left(\frac{\sigma_{inc}-\sigma_{mat}}{\sigma_{inc}+\sigma_{mat}}\frac{R^2}{r^2} - 1\right)\frac{I}{\sigma_{mat}}l_i z^i \quad \text{outside the circular inclusion} \tag{57}$$

and

$$\varphi_{inc}(z) = -\frac{2}{\sigma_{inc}+\sigma_{mat}}Il_i z^i \quad \text{inside the circle .} \tag{58}$$

Using Eqs. 57 and 58, we arrive at the following relationships for the current distribution:

a) outside the circular inclusion

$$\frac{I_k(z)}{I} = l_k - \frac{\sigma_{inc}-\sigma_{mat}}{\sigma_{inc}+\sigma_{mat}}\frac{R^2}{r^2}l_k + 2\frac{\sigma_{inc}-\sigma_{mat}}{\sigma_{inc}+\sigma_{mat}}\frac{R^2}{r^4}z_{jk}z^j z^i l_i \tag{59}$$

b) inside the circle

$$\frac{I_k(z)}{I} = \frac{2\sigma_{inc}}{\sigma_{inc}+\sigma_{mat}}l_k \quad . \tag{60}$$

In the nondimensional form we get

a) outside the circular inclusion

$$\frac{I_k(z)}{I}l^k = 1 + \frac{\Sigma-1}{\Sigma+1}\frac{R^2}{r^2}(2\cos^2\Theta - 1) \tag{61}$$

and

b) inside the circle

$$\frac{I_k(z)}{I}l^k = \frac{2\sigma_{inc}}{\sigma_{inc}+\sigma_{mat}}l_k \tag{62}$$

where $\Sigma = \frac{\sigma_{inc}}{\sigma_{mat}}$ and $\cos\Theta = \frac{1}{r}z^i l_i$.

## 5. Evaluation and Visualization of Exact Solution for Spherical Inclusion

The system with fixed current applied to a linear isotropic electroconducting material with a spherical (Eqs. 32–37) or circular-prismatic (Eqs. 57–60) inclusion lends itself well to visualization, since the exact solution has an explicit, closed form. For convenience and brevity, we choose to visualize the spherical case, with the further simplification that the fixed current imposed at the boundary is oriented along the longitudinal axis $z^1$ shown in Fig. 1. In this case, if the domain has a fixed electrical conductivity, then Ohm's law implies that boundary conditions prescribing the far-field current density $I$ at infinity are interchangeable with an ambient electric field $E_{far}$.

For purposes of visualization, we redefine the coordinate system as $z_1 \to z$ and $(z_2^2 + z_3^2)^{1/2} \to r$. We have now changed the meaning of $r$ relative to the text above, and within this axisymmetric coordinate system the radial distance from the sphere center is renamed as $\rho = \sqrt{r^2 + z^2}$. If the material conductivity is isotropic, then cylindrical symmetry is ensured. If a voltage drop is applied between the $\pm z$ ends of the domain, a steady current flows in the $z$ direction, around and across the inclusion.

The electric potential for the case of a spherical inclusion with linear isotropic materials is given in Eqs. 32 and 33. With the previous assumptions, we can rewrite $Il_i$ as $I\hat{z}$, and $Il_i z^i$ as $Iz$. Then Eqs. 32 and 33 for the electric potential can be written as

$$\varphi(r,z) = \left( \frac{\sigma_{inc}-\sigma_{mat}}{\sigma_{inc}+2\sigma_{mat}} \frac{R^3}{\rho(r,z)^3} - 1 \right) \frac{I}{\sigma_{mat}} z, \qquad \rho \geq R \qquad (63)$$

$$\varphi(r,z) = - \frac{3\sigma_{mat}}{\sigma_{inc}+2\sigma_{mat}} \frac{I}{\sigma_{mat}} z, \qquad \rho \leq R \ . \qquad (64)$$

We also define an equivalent boundary condition on the electric field at infinity, given by $E_{far} = I/\sigma_{mat}$. To simplify the notation further, we introduce field distortion factors due to the sphere's presence for radial location $\rho$ outside or inside the sphere radius $R$:

$$D_{out} = \frac{\sigma_{inc}-\sigma_{mat}}{\sigma_{inc}+2\sigma_{mat}} \qquad (65)$$

$$D_{in} = \frac{3\sigma_{mat}}{\sigma_{inc}+2\sigma_{mat}} \qquad . \qquad (66)$$

Then, we have the following equations:

11

$$\varphi(r,z) = \left(D_{out}\frac{R^3}{\rho^3} - 1\right)E_{far}z, \qquad\qquad \rho \geq R \qquad (67)$$

$$\varphi(r,z) = -D_{in}E_{far}z, \qquad\qquad\qquad \rho \leq R \quad . \qquad (68)$$

Similarly, Eqs. 34 and 35 for the electric field can be rewritten. The $z_{im}$ appearing in Eq. 34 is equivalent to the Kronecker delta function. For our axisymmetric geometry and current oriented along $\hat{z}$, we can rewrite the quantity $z_{im}z^m z^k l_k$ in Eq. 34 as $z^2\hat{z} + zr\hat{r}$. We also shift from indicial notation to vector notation. Thus, we have

$$\vec{E}(r,z) = \left(1 - D_{out}\frac{R^3}{\rho^3}\right)E_{far}\hat{z} + 3D_{out}\frac{R^3}{\rho^5}E_{far}(z^2\hat{z} + zr\hat{r}), \qquad \rho > R \qquad (69)$$

$$\vec{E}(r,z) = D_{in}E_{far}\hat{z}, \qquad\qquad\qquad\qquad \rho < R \quad . \quad (70)$$

If we define a unit vector $\hat{\rho}$ in the radial direction relative to the sphere center, then Eq. 70 can also be written conveniently in nondimensional form as

$$\frac{\vec{E}(r,z)}{E_{far}} = 1 + D_{out}\frac{R^3}{\rho^3}\left(-\hat{z} + 3\frac{z}{\rho}\hat{\rho}\right), \qquad \rho > R \quad . \qquad (71)$$

Finally, for the current density field, we can make similar substitutions in Eqs. 36 and 37 to obtain

$$\vec{I}(r,z) = \left(1 - D_{out}\frac{R^3}{\rho^3}\right)\sigma_{mat}E_{far}\hat{z} + 3D_{out}\frac{R^3}{\rho^5}\sigma_{mat}E_{far}(z^2\hat{z} + zr\hat{r}), \quad \rho > R \quad (72)$$

$$\vec{I}(r,z) = D_{in}\sigma_{inc}E_{far}\hat{z}, \qquad\qquad\qquad\qquad \rho < R \quad . \quad (73)$$

We note that inside the spherical inclusion ($\rho < R$), these conditions hold:

- The electric potential is a function of $z$ only.

- The electric field and current density are uniform and oriented in the $\hat{z}$-direction only.

Distances in this problem scale with $R$, so we choose $R = 1$ m as the inclusion radius for our visualization. We then apply an electric field at infinity $E_{far} = 100$ V/m oriented in the $+z$ direction (+ voltage on the left, – voltage on the right), and plot the solution over a spatial domain with a width equal to several sphere radii in each direction. The two extreme configurations are plotted in Fig. 2: a strongly insulating inclusion ($\sigma_{inc} \ll \sigma_{mat}$) and a strongly conducting inclusion ($\sigma_{inc} \gg \sigma_{mat}$). The matrix conductivity is $\sigma_{mat} = 1$ S/m in both cases. An insulating inclusion is modeled by $\sigma_{inc} = 10^{-9}$ S/m, a conductor by $\sigma_{inc} = 10^{+9}$ S/m.

For an insulating sphere included in a relatively electroconducting medium, the field-distortion factors asymptote to their limits: $D_{out} \rightarrow -0.5$ and $D_{in} \rightarrow 1.5$. This implies that the electric field inside the insulating inclusion asymptotes to $1.5\ E_{far}$. Electric field lines will tend to diverge or bulge around the inclusion, while equipotential lines (contours of $\varphi$), which are everywhere normal to the electric field, will tend to be pulled into the sphere. The analytic solution for this configuration is plotted in Fig. 2a. Equipotentials are shown as curves colored by the magnitude of $\varphi$. The electric field is indicated by red arrows whose length is proportional to the field magnitude.

For a conducting sphere included in a relatively insulating matrix, the field-distortion factors asymptote to their limits: $D_{out} \rightarrow 1$ and $D_{in} \rightarrow 0$. This implies that the electric potential and electric field inside the conducting inclusion both asymptote to zero. Electric field lines will tend to converge into the inclusion, while equipotential lines will tend to be pushed out of the inclusion. The analytic solution for this configuration is plotted in Fig. 2b
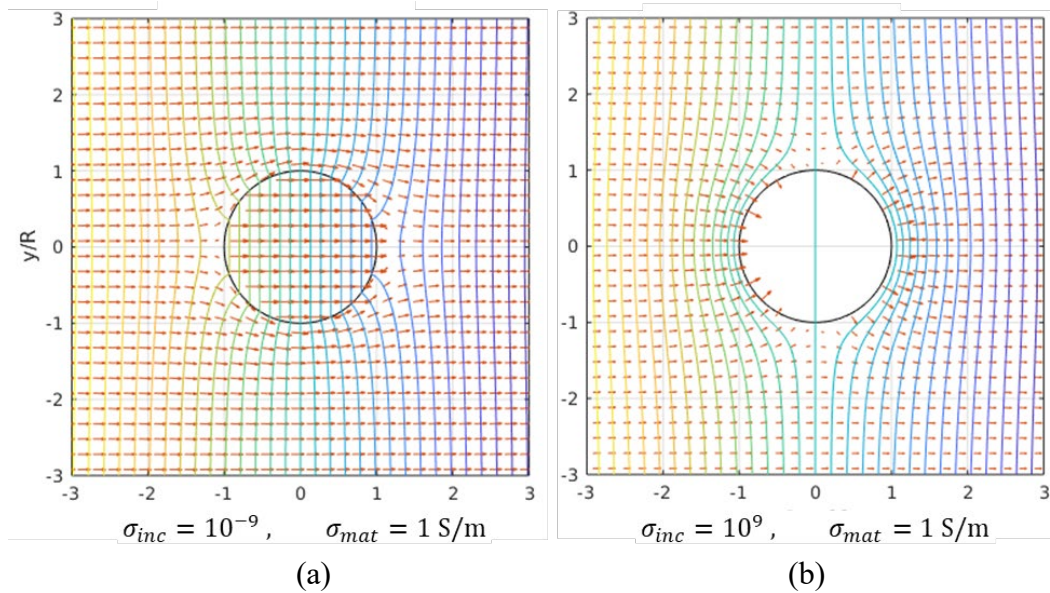


**Fig. 2    Equipotential lines and electric field vectors for the analytic solution given in Eqs. 67–70 for a) a strongly insulating inclusion and b) a strongly conducting inclusion**

For both of these scenarios, the analytic solution shows a region of field distortion around the inclusion, with a uniform, horizontal field inside the inclusion that is enhanced with respect to the far field by the insulating inclusion and suppressed by the conducting inclusion. The region of visible field distortion extends to a few radii outside the inclusion. There is a nonzero distortion of the field even at very great distances from the inclusion. Equations 40 and 71 indicate this distortion falls off

13

as $\rho^{-3}$. Evaluating the solution at $z = 10R$, we calculate that the nominal equipotential curve shifts by less than $R/1000$.

## 6. Finite-Element Simulation Setup

For the case of linear isotropic materials inside and outside the inclusion, the finite-element electromagnetics simulation code ALEGRA can be used to compute approximate solutions to this problem. The computed solutions for a spherical inclusion can be compared directly with the closed-form solutions appearing in Eqs. 32–37, restated in Eqs. 63–73. This serves two purposes: 1) to verify the exact solutions computed here are consistent with those generated numerically and 2) to provide the groundwork for future verification of ALEGRA and codes like it for this class of problems.

As described in Grinfeld et al.,[10] Grinfield and Niederhaus,[11] and Robinson et al.,[14] ALEGRA is a multiphysics, multimaterial finite-element simulation code that can be used to model resistive magnetohydrodynamics and electromechanics in two or three dimensions (2-D or 3-D). Similar to the previous verification studies in Grinfeld et al.[10] and Grinfeld and Niederhaus,[11] here we use only the "transient magnetics" module from the 3-D electromagnetics portion of the code, leaving any concept of material motion or mechanics out of the simulation. In this portion of ALEGRA, the transient eddy-current diffusion equation is solved using implicit time integration on a 3-D mesh of hexahedral finite elements. The spatial discretization places magnetic flux on element faces and electric field circulation on elements edges, forming a "mimetic" or "compatible" discretization that allows the physical and mathematical properties of Maxwell's laws to be preserved more rigorously. This discretization has been described and evaluated extensively elsewhere.

The simulation is created as an initial boundary value problem in Cartesian $(x, y, z)$ space. The problem is rotated such that the far-field electric field and current density lie along the $x$-axis. At time zero, the electric current is zero everywhere. The electrical conductivity $\sigma$ is specified everywhere in the domain, associated with the local material composition. The $x = 0$ plane of symmetry is defined as ground ($\varphi = 0$), and a fixed driving voltage $\varphi_0 = -E_{far} x_{max}$ is applied to the maximum $x$ boundary for all time. On these specified-voltage surfaces, the electric field is constrained to be everywhere normal to the boundary: $\vec{E} \times \hat{n} = 0$. These boundaries are shown below in Fig. 3a as gray-shaded surfaces. On the lateral $(-y, +y, -z, +z)$ boundary surfaces, the electric field is constrained to be tangent to the boundary: $\vec{E} \cdot \hat{n} = 0$. These boundaries are unshaded in Fig. 3a.
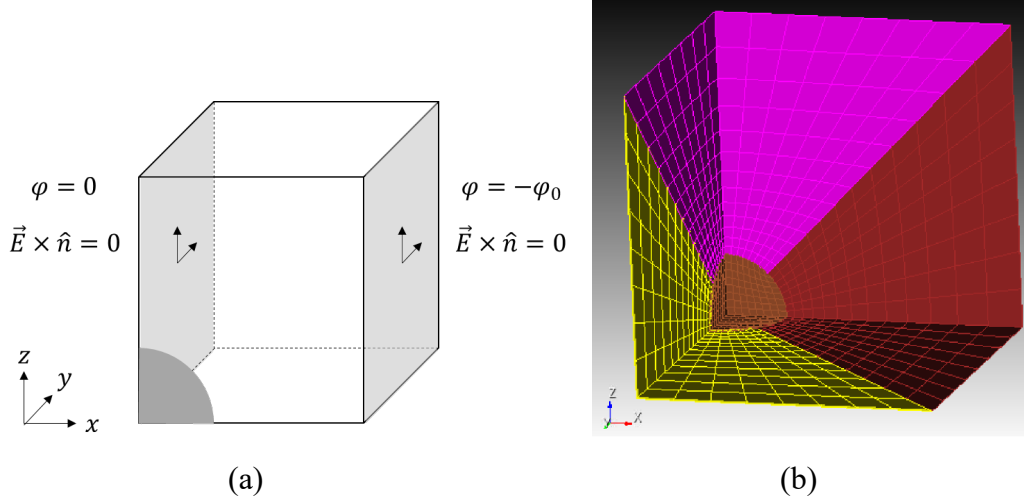
**Fig. 3    a) ALEGRA simulation domain configuration and boundary conditions, with symmetry imposed and fixed-voltage boundaries shown in gray; b) simulation mesh configuration's net current flow and voltage gradient are oriented in the $+x$ direction**

With exterior boundaries sufficiently far from the inclusion, this sets up a uniform electric field equal to $E_{far}$ outside the region distorted by the inclusion. The simulation starts up and runs until a stationary flow of current is reached, and this solution is compared with the analytic solution described previously. A constant time-step size of 0.5 μs is used, but for the insulating case the stationary state is reached in less than one time step.

Two simplifications are made to the model here. First, we apply the "low magnetic Reynolds number" ("low $R_m$") approximation in ALEGRA.[15–17] In this approximation, the contribution to the current density due to a time-changing magnetic field is assumed to be small relative to the contribution due to the electric-field gradient. The magnetic field can then be dropped from the system completely, and instead of the eddy-current diffusion equation, only this equation is solved on each time step:

$$\nabla \cdot \sigma \nabla \varphi = 0 \quad . \tag{74}$$

This equation is much less computationally expensive to solve and allows the use of more convenient electric-potential boundary conditions ("potential drive") for the present case. Without this approximation, boundary conditions on the magnetic field would be required, and this would imply the need for a magnetized space outside the conducting region. Applying this approximation does not eliminate the possibility to study the effect of Joule heating, which is still included in the model.

The second simplification is that axial and lateral symmetry is applied when choosing the domain for simulation. The "low $R_m$" approximation is only available

in 3-D in ALEGRA, so the simulation cannot take advantage of the inherent axisymmetry of the problem. Instead, symmetry about all three coordinate-aligned midplanes of the spherical inclusion is assumed. Thus, the simulation domain need only enclose a one-eighth sector of the insulating sphere inclusion, along with the conducting region extending out to one of the voltage boundaries. This configuration of the simulation domain in shown in Fig. 3a.

A hexahedral mesh is generated for the simulation, with block boundaries conforming to the spherical surface of the inclusion, and all elements thus containing only pure material. No mixed-material elements are included. A coarse version of this mesh is shown in Fig. 3b. To make the boundary geometry consistent with the selected $\vec{E} \times \hat{n} = 0$ boundary conditions on the electric field, the $+x$ boundary of the mesh is additionally made conformal to equipotential curves from the exact solution, and the $+y$ and $+z$ boundaries are made conformal to the electric field lines from the exact solution. These adjustments to the mesh are on the order of microns in magnitude for the geometry used here. They are not visible in this macroscopic view of the mesh, where the boundaries appear to be flat. But analysis (not included here) has shown that these adjustments eliminate boundary errors that would otherwise be comparable in magnitude to the interior errors for sufficiently high resolution. Without them, a prohibitively large distance is required between the exterior boundaries and distorted-field region around the inclusion.

## 7. Finite-Element Solution

Using the mesh and simulation settings described in Section 6, an ALEGRA simulation is performed for the insulating inclusion case. We use a sphere radius $R = 1\,\text{m}$ and a driving voltage $\varphi_0 = -5E_{far}R = -500$ V, with all exterior boundaries located at a distance of 5 inclusion radii (5 m) from the origin. This effectively imposes an exterior electric field $E_{far} = 100$ V/m. The sphere and exterior conductivities are $10^{-9}$ and 1.0 S/m, respectively.

The mesh resolution is designated by the number of elements $N$ spanning the sphere radius. A linear bias extends outward from the sphere surface to the boundaries. The mesh shown in Fig. 3b is for $N = 8$ for simplicity, but calculations are performed for resolution as high as $N = 64$.

The results of the ALEGRA simulation at $N = 64$ are shown in Fig. 4. In this view, the simulation domain is shown only on the $z = 0$ plane, and then reflected about the symmetry planes in order to visualize four parameters of the solution. Included in this plot is the volumetric rate of Joule heating, $\vec{J} \cdot \vec{E}$. This quantity has units of power per unit volume, and it describes the rate at which heat is deposited locally due to current flow through material with finite conductivity. The ALEGRA

16

simulation here is done with Joule heating disabled, to preserve the stationary nature of the final solution. (Thermal conduction is also excluded.) Instead, $\vec{I} \cdot \vec{E}$ is computed here as a postprocessing step for comparison with the analytic solution.
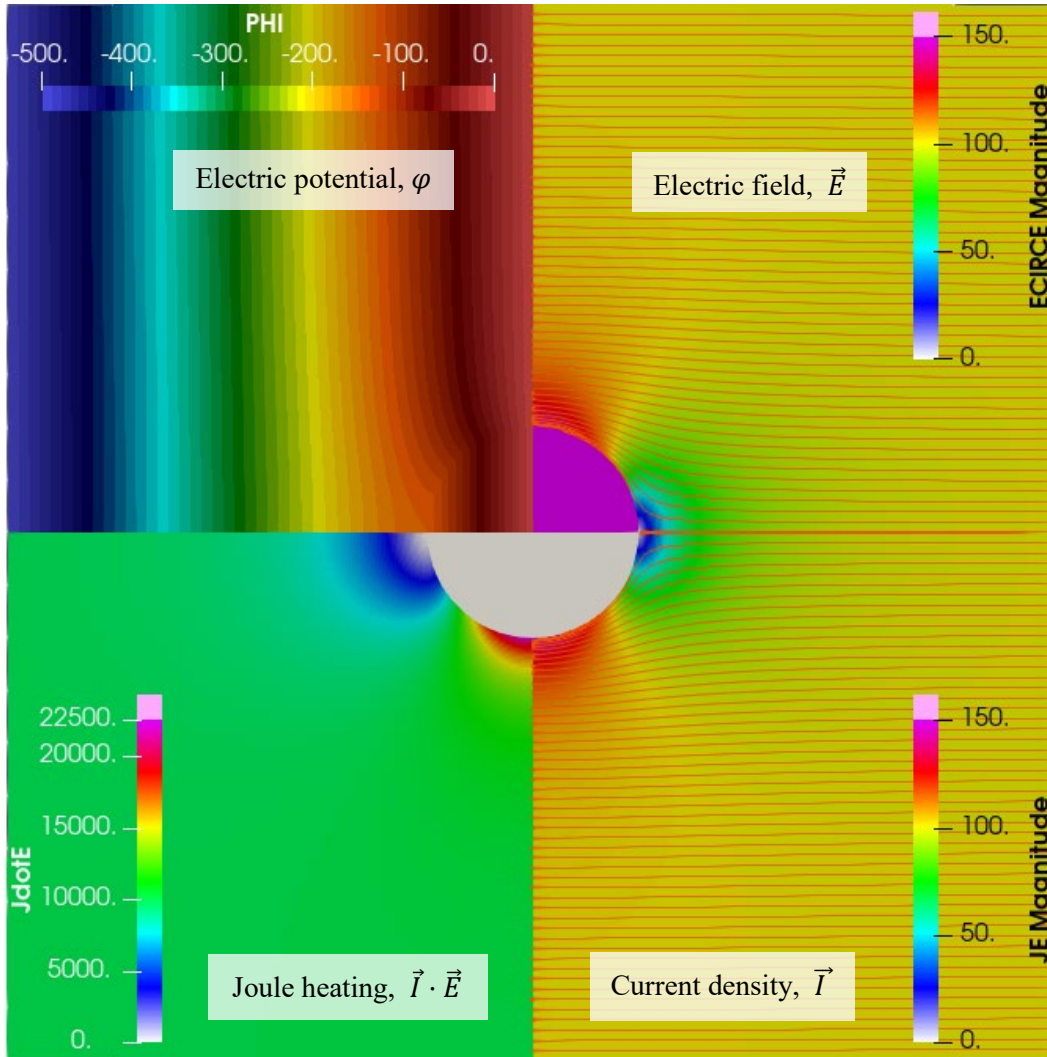


**Fig. 4** **ALEGRA solution computed for the insulating-sphere case with $R = 1$ m, $E_{far} = 100$ V/m, $\varphi_0 = -500\,V$, and $N = 64$ elements spanning the sphere radius**

Shown in Fig. 4 are these variables from the ALEGRA simulation (in clockwise order from the top left): electric potential $\varphi$, electric field magnitude $|\vec{E}|$, currentdensity magnitude $|\vec{I}|$, and rate of Joule heating, $\vec{I} \cdot \vec{E}$. (These are noted as PHI, ECIRCE Magnitude, JE Magnitude, and JdotE in the figure.) For the electric field and current density, streamlines of the vector fields are overlaid as well. For the electric potential, a discrete stepped color mapping is used so that equipotential lines are visible as boundaries among color gradations.

As expected, the ALEGRA solution shows the same qualitative features as the analytic solution for the insulating case, with electric field lines diverging around the inclusion and equipotential lines bunching up in the vicinity. We also see that within the insulating inclusion, the electric potential is a function of $x$ only, and the electric field and current density are uniform—as expected from the analytic solution discussed previously. We have confirmed that, under refinement of the mesh, the interior electric-field magnitude and the maximum exterior value approach the analytical value of $1.5E_{far} = 150$ V/m. We also observe that the Joule heating is concentrated in a region immediately exterior to the "equator" of the spherical inclusion, where the maximum volumetric Joule heating power in the simulation is found to be $\sigma|\vec{E} \cdot \vec{E}| = 1.0 \times 150 \times 150 = 22.5$ kW/m$^3$.

Finally, pointwise errors are computed in the ALEGRA solution with respect to several variables from the analytic solution described above for the spherical insulating inclusion. The local difference with respect to the analytic values, normalized by the far-field value, is shown in Fig. 5 for the following variables, laid out in clockwise order (like Fig. 4) from the top left: electric potential $\phi$, electric field magnitude $|\vec{E}|$, current density magnitude $|\vec{I}|$, and rate of Joule heating, $\vec{I} \cdot \vec{E}$. We see the maximum errors are on the order of $10^{-4}$ or 0.01% for $N = 64$, and these are concentrated near the material interface. For the electric field and the electric potential, smaller but still significant errors are present in the sphere interior. Further, in analysis not shown here, we found that for the electric field and current density, the errors decay as $1/N^2$ under refinement of the mesh.
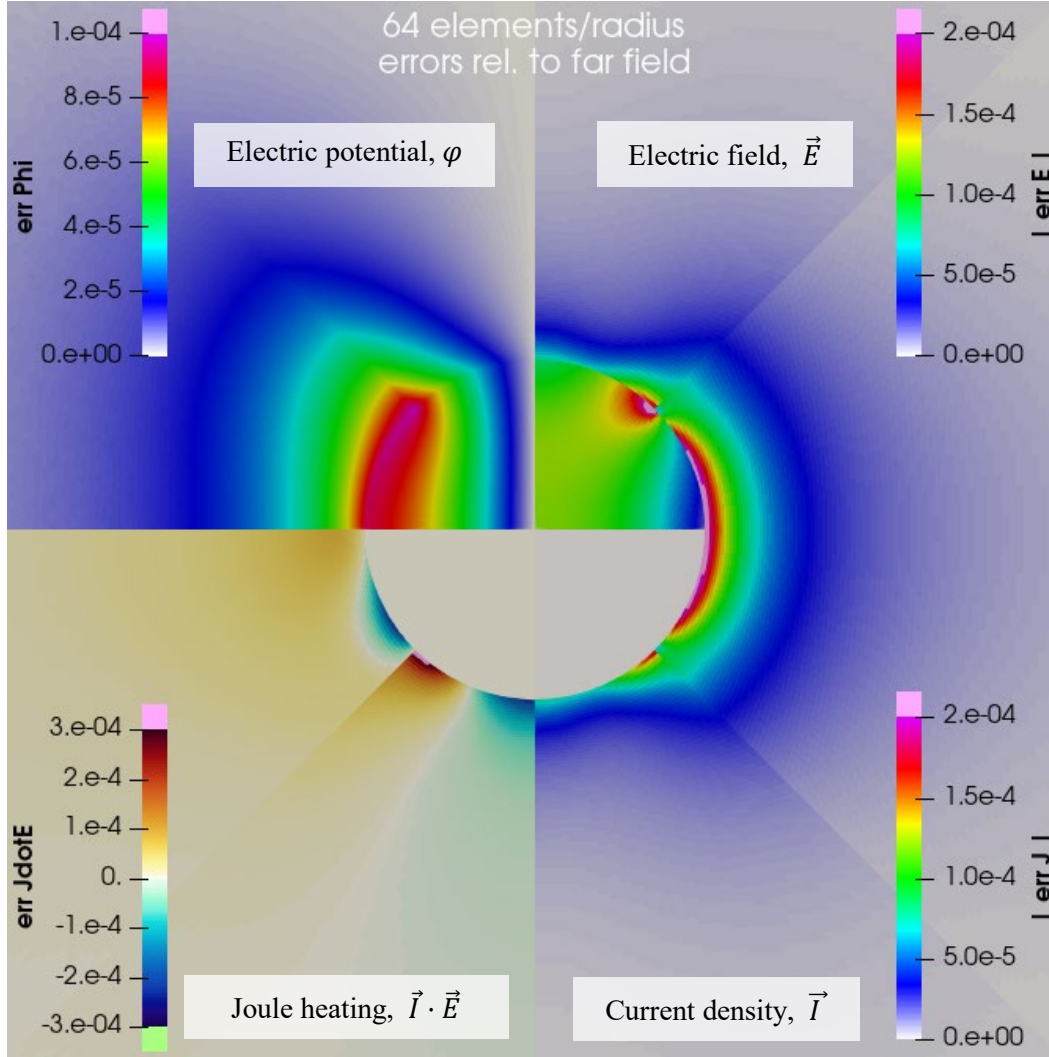
**Fig. 5**   **Fractional error in ALEGRA solution computed for the insulating-sphere case with $R = 1$ m, $E_{far} = 100\ V/m$, $\varphi_0 = -500\ V$, and $N = 64$ elements spanning the sphere radius; fractional error is computed relative to the analytic value and normalized to the far-field value**

There are significant errors in the Joule heating, and they can have either sign: overheating or underheating. But, they are preferentially located in the conducting material near the interface. The presence of these errors is remarkable for several reasons. On one hand, these errors are expected because ALEGRA does not allow for the natural interface conditions on the normal and tangential components of the electromagnetic fields to be imposed locally in the domain interior. This was also observed and discussed in Grinfield and Niederhaus.[11] (Such conditions would be impractical for magnetohydrodynamic [MHD] simulations with motion, particularly for Eulerian meshes.) On the other hand, in that work[11] these errors were attributed to mixed-material elements. But in this mesh, there are no mixed-material elements. Thus, we observe that even with pure materials, and a mesh that

is conformal to interfaces, there are nonzero errors in the local rate of Joule heating. In MHD simulations that couple electromagnetic fields to the dynamics and thermodynamics of moving media, these errors could produce significant anomalies, particularly if the local heating can affect the local electrical conductivity, which may lead to very large, localized, and possibly spurious rates of heating or cooling.

This comparison to analytic solutions is being extended to the conducting sphere case, to rectangular meshes with mixed-material elements, and to other simulation options, including advanced Joule heating variants. The analysis lends itself well to rigorous verification, since spatial norms of the errors shown in Fig. 5 could be incorporated into a convergence study with respect to mesh refinement. These error norms would need to account for subgrid variation of both the finite-element solution and the exact solution, which could be challenging, particularly when mixed-material elements are present. But convergence rates for the various ALEGRA simulation configurations could be studied, providing a quantitative basis for use of these options in ALEGRA simulations for other applications.

## 8. Conclusion

We applied the Eshelby technique to the exact analysis of the steady-state electric current in the unbounded linear isotropic matrix containing a spherical inclusion. Contrary to the matrix, the uniform inclusion can be anisotropic and even nonlinear.

Even in this multimaterial domain, the technique allowed us to obtain a relatively simple, closed-form analytic solution for the case of linear isotropic material in the inclusion that allows us to study Joule heating in particular. Simulations with the ALEGRA code for one realization of the problem agreed with the analytical solution to within $10^{-4}$ relative to the far-field values. This was true for all four variables studied, including the rate of Joule heating.

While this agreement is very close, we also note that the mesh used in the ALEGRA simulation was body-fitted, and for engineering calculations it may not be possible to use a conformal body-fitted mesh. The closed-form analytic solutions generated here provide a convenient groundwork for future verification of ALEGRA simulations that do not benefit from body-fitted meshes, which should allow a clearer understanding of the nature and magnitude of Joule heating errors for those situations to be gained.

## 9.    References

1. Cooper PW. Exploding bridgewire detonators. Explosives engineering. Hoboken (NJ): Wiley-VCH; 1996. p. 353–367.

2. Hansen S. Exploding wires principles, apparatus and experiments. The Bell Jar; 2011.

3. Doney RL, Vunni GB, Niederhaus JHJ. Experiments and simulations of exploding aluminum wires: validation of ALEGRA-MHD. Aberdeen Proving Ground (MD): Army Research Laboratory (US); 2010 Sept. Report No.: ARL-TR-5299.

4. Zellner MB, Doney RL, Uhlig WC, Berning P, Bartkowski P, Halsey S. Concept for spatial visualization of magnetic fields from exploding wires. Aberdeen Proving Ground (MD): CCDC Army Research Laboratory (US); 2019 June. Report No.: ARL-TR-8706.

5. Landau LD, Lifshitz EM. Electrodynamics of continuous media. Oxford, United Kingdom: Pergamon Press; 1960.

6. Сретенский ЛН [Sretenskii LN]. Теория Ньютоновского Потенциала [Theory of Newtonian potential]. Russian; 1942.

7. Carslaw HS, Jaeger JC. Conduction of heat in solids. Oxford, United Kingdom: Oxford Science Publications; 1959.

8. Eshelby JD. The determination of the elastic field of an ellipsoidal inclusion, and related problems. Proc Royal Soc A. 1957;241(1226):376–396.

9. Eshelby JD. The elastic field outside an ellipsoidal inclusion. Proc Royal Soc A. 1959;252(1271):561–569.

10. Grinfeld M, Niederhaus J, Porwitzky A. Using the ALEGRA code for analysis of quasi-static magnetization of metals. Aberdeen Proving Ground (MD): Army Research Laboratory (US); 2015 Sep. Report No.: ARL-TR-7415.

11. Grinfeld M, Niederhaus J. ALEGRA-MHD simulations for magnetization of an ellipsoidal inclusion. Aberdeen Proving Ground (MD): Army Research Laboratory (US); 2017 Aug. Report No.: ARL-TR-8092.

12. Elliott CM, Larsson S. A finite element model for the time dependent Joule heating problem. Math Comp. 1995;64(212):1433–1453.

13. Rienstra SW. Geometrical effects in a Joule heating problem from miniature soldering. J Eng Math. 1997;32:59–80.

14. Robinson AC, Brunner TA, Carroll S, Drake R, Garasi CJ, Gardiner T, Haill T, Hanshaw H, Hensinger D, Labreche D, et al. ALEGRA: an arbitrary Lagrangian-Eulerian multimaterial, multiphysics code. Proceedings of the 46th AIAA Aerospace Sciences Meeting and Exhibit; 2008 Jan 7–10; Reno, NV. Paper No.: AIAA-2008-1235.

15. Robinson AC, Petney SV, Garasi CJ. A low magnetic Reynolds number approximation for MHD modeling. Albuquerque (NM): Sandia National Laboratories (US); 2013. Unpublished draft report.

16. Robinson AC, Drake RR, Luchini CB, Petney SV. Electromagnetic continuum mechanics in ALEGRA. Albuquerque (NM): Sandia National Laboratories (US); 2016. Unpublished manuscript.

17. Siefert C. Low rm MHD for Alexa in one page. Albuquerque (NM): Sandia National Laboratories; 2017. Unpublished draft memo.

## List of Symbols, Abbreviations, and Acronyms

| | |
|---|---|
| 2-D | 2-dimensional |
| 3-D | 3-dimensional |
| ALEGRA | Arbitrary Lagrangian-Eulerian General Research Application |
| MHD | magnetohydrodynamic |